Applied Surface Science 407 (2017) 282–296

Contents lists available at ScienceDirect

Applied Surface Science

journal homepage: www.elsevier.com/locate/apsusc

Full Length Article

# Insight into size dependence of $C_2$ oxygenate synthesis from syngas on Cu cluster: The effect of cluster size on the selectivity

Riguang Zhang[a,b], Mao Peng[a], Tian Duan[a], Baojun Wang[a,*]

[a] Key Laboratory of Coal Science and Technology of Ministry of Education and Shanxi Province, Taiyuan University of Technology, Taiyuan 030024, Shanxi, PR China

[b] Department of Chemical and Petroleum Engineering, The University of Wyoming, Laramie, WY 82071, USA

ARTICLE INFO

*Article history:*
Received 21 August 2016
Received in revised form 28 January 2017
Accepted 18 February 2017
Available online 24 February 2017

*Keywords:*
Syngas
$C_2$ oxygenates
Cu cluster
Size effect
Selectivity
Density functional theory

ABSTRACT

Size dependence of $C_2$ oxygenate formation from syngas on Cu cluster has been investigated to qualitatively probe into the effect of Cu cluster size on the selectivity of $C_2$ oxygenates, which includes two key steps: $CH_x$ and $C_2$ oxygenate formations; $Cu_{13}$, $Cu_{38}$ and $Cu_{55}$ clusters have been employed to model different sizes of Cu cluster. Here, density functional theory method has been performed. Our results show that the adsorption ability of the species involving in $C_2$ oxygenate formation decreases with the increasing of Cu cluster size; Cu cluster size significantly affects the dominant existence forms of $CH_x(x = 1–3)$ species and $C_2$ oxygenates. Among three Cu clusters, $Cu_{13}$ cluster exhibits the highest selectivity toward $C_2$ oxygenates compared to other two clusters, suggesting that Cu cluster size can affect the selectivity toward $C_2$ oxygenates, moreover, the smaller Cu cluster size is, the higher the selectivity of $C_2$ oxygenates is. That is probably related to the high concentration of low-coordinated defect sites on small size Cu cluster, which results in the higher activity and selectivity toward $C_2$ oxygenates. The identification of higher intrinsic selectivity of $C_2$ oxygenates, active sites, and stronger cluster size effect would be valuable for developing more efficient and stable Cu catalyst with higher selectivity toward $C_2$ oxygenate in syngas conversion.



## 1. Introduction

It is well-known that syngas conversion to $C_2$ oxygenates (typically referred to as ethanol, etc.) has become an important industrial process for the production of clean liquid energy fuels and valuable chemical feedstock, however, the low yield and poor selectivity of $C_2$ oxygenates are the major hurdles associated with the use of catalysts [1–3]. Thus, it is significantly essential to develop the catalysts with higher yield and selectivity of $C_2$ oxygenates from syngas.

Four types of catalysts, Cu-based catalysts, Rh-based catalysts, modified Fischer-Tropsch catalysts and Mo-based catalysts [4–7], have been studied for syngas conversion to $C_2$ oxygenates, among them, Rh-based catalysts directly convert syngas to $C_2$ oxygenates, however, the major barrier to its large-scale application is their prohibitive cost [6,8]. Nowadays, Cu-based catalysts, as an industrial catalysts, have become an attractive option to produce $C_2$ oxygenates from syngas at the pressures of about 40–100 bar in the temperature range of 280–310 °C [9–14].

Recently, size-selected subnanometer transition metal clusters have received considerable attention in catalysis due to their unique electronic and catalytic properties, which are different from bulk metal surfaces and larger nanoparticles [15–19]. Since both the size and the coordination numbers of the nanoparticle are different from those of bulk metal surface, both can significantly affect the chemical reactivity. Especially, for the metal nanocluster, an up-shift of the average energy for *d*-electron states originates from the finiteness of cluster size, thus, the higher average energy of *d*-electron states leads to the higher catalytic activity and the stronger interaction of cluster with the adsorbed species [16]. Moreover, the catalytic activity of metal cluster depends on the cluster size, for example, the reactivity of Au cluster increases with the decreasing of cluster size [20]. Fajín et al. [21] have discussed the effects of Pt cluster size and structure on the homolytic $H_2O$ dissociation on Pt clusters (n = 13, 19, 38, 55, 79 and 140), suggesting that the activation barrier increases with the increasing of cluster size. Xie and Gong [22] have studied the interaction of $Au_{55}$ cluster with small molecules CO and $O_2$, indicating that the $Au_{55}$ cluster can enhance the reaction process, $CO + O_2 \rightarrow CO_2 + O$, in which the reaction barrier is only about half electron volts. In addition, Rösch and co-workers [23–25] have investigated CO adsorption on Pt and

* Corresponding author at: No. 79 Yingze West Street, Taiyuan 030024, PR China.
*E-mail addresses:* wangbaojun@tyut.edu.cn, quantumtyut@126.com (B. Wang).

http://dx.doi.org/10.1016/j.apsusc.2017.02.164
0169-4332/

Pd clusters, and obtain the effect of cluster size on CO adsorption properties.

For Cu cluster, Knickellbein [26] experimentally found that the ionization of $Cu_n$ up to 150 atoms corresponds to the electronic shell and subshell closings. Kostko et al. [27] obtained that $Cu_{38}$ cluster is an oblate structure by photoelectron spectroscopy. Zhang and co-workers [28] examined the structures and binding energies of Cu clusters (n = 2–70,147,500) using Monte Carlo and Embedded-Atoms Method, suggesting that Cu clusters (n = 2–70) are formed by gradually increasing atoms to the icosahedral surface at 300 K; moreover, the higher the symmetry is, the more stable Cu cluster is. Meanwhile, Winter et al. [29] presented the evidence that small Cu clusters showed both the jellium-like electronic behavior and icosahedral geometrical structure. The experimental studies by Lu et al. [30] have synthesized the stable $Cu_8$ and $Cu_{13}$ nanocluster.

On the other hand, Cu nanocluster has exhibited the remarkable catalytic activity [15,31–38], DFT studies by Fernández et al. [15] have shown that the barrier of $O_2$ dissociation decreases with the increasing of cluster atomicity on $Cu_n$(n = 3–8,13,38) clusters. First-principles calculations by Lee et al. [32] have proved that a $Cu_{38}$ cluster exhibits the higher catalytic selectivity for ethylene epoxidation compared to $Au_{38}$ cluster. Liu et al. [34] have experimentally obtained that $Cu_4$ cluster supported on $Al_2O_3$ exhibits the highest activity for $CO_2$ hydrogenation to $CH_3OH$ at a low $CO_2$ partial pressure, namely, small Cu cluster is the excellent and efficient catalyst. DFT studies by Yang et al. [35] show that $Cu_{29}$ cluster presents a higher activity than Cu(111) surface for CO hydrogenation to methanol. Zuo et al. [36] investigated the effect of Cu cluster size on $CH_3OH$ dissociation using DFT calculations, suggesting that the effect of cluster size is beneficial for $CH_2O$ dehydrogenation, which inhibits $CH_2O$ desorption as a by-product. Liu and Rodriguez [37] investigate the water-gas-shift reaction on $Cu_{29}$ cluster and Cu(100) surfaces, suggesting that the WGS activity of $Cu_{29}$ is higher than that of Cu(100) surface, which agrees well with the experimental observations. Further, $CO_2$ adsorption and activation over medium sized $Cu_n$(n = 7, 13 and 19) clusters [39], methanol decomposition on $Cu_4$ clusters [40], and the size dependence of the adsorption energy for sulfur on (111) facets of tetrahedral Cu clusters up to sizes of ~300 atoms [41] have been systematically examined using DFT calculations.

Up to now, to the best of our knowledge, the understanding about the underlying mechanism of $C_2$ oxygenate formation from syngas on Cu cluster, as well as the size effect of Cu cluster on the catalytic performance of $C_2$ oxygenate formation remains unelucidated theoretically at a molecular level. As a result, in order to search the novel Cu-based catalyst with the improved catalytic activity and selectivity toward $C_2$ oxygenates, it is necessary to probe into $C_2$ oxygenates formation from syngas on different size of Cu clusters, and further identity the size effect of Cu cluster on the catalytic performance of $C_2$ oxygenates.

In this study, $Cu_{13}$, $Cu_{38}$ and $Cu_{55}$ cluster models have been employed to represent different sizes of Cu cluster. Then, the adsorptions of all possible species involved in $C_2$ oxygenate formation have been examined on three Cu clusters. Further, the effect of by-product (methanol and methane) on the selectivity of $C_2$ oxygenates has been discussed in detail. Finally, the obtained results may provide some information for the design and optimization of highly-efficient Cu-based catalysts in $C_2$ oxygenate formation from syngas.

## 2. Computational details

### 2.1. Computational method

All DFT calculations have been performed using Dmol$^3$ program package in Materials Studio 4.4 [42,43], where the generalized gradient approximation (GGA) with the Perdew-Wang exchange–correlation functional (PW91) are employed, which has been widely used for the calculations of cluster models and the studies about syngas conversion, moreover, the obtained results are often reliable [44,45]. In the computation, the double-numerical basis set with a polarization *d*-function (DNP) is chosen to expand the valence electron functions. The orbital cutoff range is 4.0 Å, and the smearing value is set to be 0.005 hartree. The inner electrons of Cu atoms are kept frozen and replaced by an effective core potential (ECP), and other atoms are treated with all-electron basis set.

In order to determine the accurate activation barrier of the reaction, the complete LST/QST approach is used to search the transition state of the reaction [46,47]. Frequency analysis has been used to validate the transition state with only one imaginary frequency; moreover, TS confirmation is also performed on every transition state to confirm that they lead to the desired reactants and products [48]. The reaction energy ($\Delta E$), activation barrier ($E_a$) and adsorption energy ($E_{ads}$) with zero-point vibrational energy (*ZPE*) corrections [21] are obtained; the detailed descriptions are presented in the Supplementary material.

### 2.2. Surface model

In the calculation, the structural stability of nanocluster is a key factor [49]. For Cu cluster, many isomers exist, and the number of cluster isomer increases rapidly with the increasing of cluster size. In this study, $Cu_{13}$, $Cu_{38}$ and $Cu_{55}$ nanoparticles with the measuring diameters of 5, 8 and 10 Å have been employed to investigate the effect of Cu cluster size on $C_2$ oxygenate formation. Fig. 1 presents the most stable configurations of $Cu_{13}$, $Cu_{38}$ and $Cu_{55}$ clusters.

Although a face centered cubic structure is the most stable structure of bulk Cu, another icosahedron structure with five-fold symmetry has been found in nano-sized systems. It is well-known that Cu(111) surface has the lowest surface energy; in order to decrease the surface energy, an icosahedron structure with five-fold symmetry is formed including twenty (111) surfaces. Meanwhile, for $Cu_{13}$ cluster, previous studies [15,49–55] have shown that for a 13-atom Cu nanocluster, the icosahedron structure is the most stable than other isomers; thus, $Cu_{13}$ cluster with the icosahedron structure has been considered (see Fig. 1(a)), which is a core-shell structure with 12 atoms in outer shell and an atom in core shell; moreover, all the shell atoms have the same coordination number 6, thus only three adsorption sites exist: Top, Bridge and Hcp.

For $Cu_{38}$ clusters, the truncated octahedron structure for the fcc lattice is more stable than other isomers, which is identified by previous studies [15,53–60]. Fig. 1(b) presents $Cu_{38}$ clusters with an outer shell of 32 atoms and a core shell of 6 octahedral atoms, moreover, the outer shell has 8 atoms at the center of (111) facet and 24 atoms on (100) facet. Due to outer shell atoms with the coordination number 6 and 9, $Cu_{38}$ cluster has eight adsorption sites: Top I, Top II, Bridge I, Bridge II, Bridge III, Fcc, Hcp and Hollow. Top I is the vertex of (100) facet and in six coordination with five atoms on the outer shell and one atom in the core shell. Top II is the center of (111) facet and in nine coordination with six atoms on the outer shell and three atoms in the core shell. Other adsorption sites are formed on the basis of Top I and Top II sites.

For $Cu_{55}$ cluster, the highly symmetric structure holds the obvious predominance in isomers, the icosahedron $Cu_{55}$ cluster is the most stable structure, which is also identified by previous studies [30,53,54,61–64]. As shown in Fig. 1(c), $Cu_{55}$ cluster comprises three shells with an outer shell of 42 atoms, second shell of 12 atoms and a core atom; moreover, the outer shell corresponds to (111) facet. Similarly, the outer shell atoms of $Cu_{55}$ cluster has the coordination number 6 and 8, thus, $Cu_{55}$ cluster has six adsorption sites: Top I, Top II, Bridge I, Bridge II, Fcc and Hcp. Top I is the

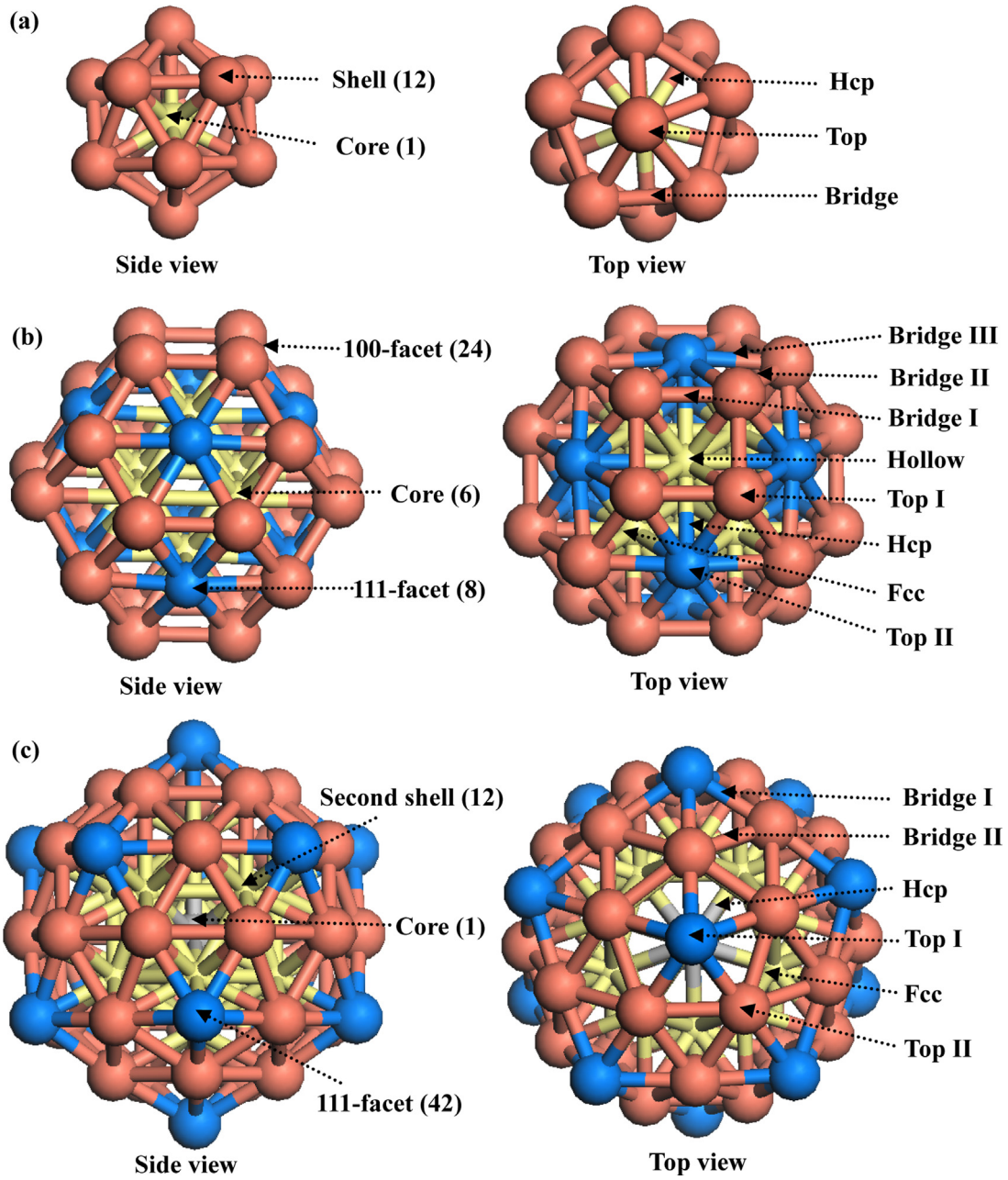


**Fig. 1.** The side and top views of (a) $Cu_{13}$ cluster, (b) $Cu_{38}$ cluster, and (c) $Cu_{55}$ cluster.

vertex of the icosahedron and in six coordination, whereas Top II is in eight coordination; Other adsorption sites are formed on the basis of the Top I and Top II sites.

## 3. Results and discussion

### 3.1. Adsorption of all possible species in $C_2$ oxygenate formation

The adsorptions of all species involved in $C_2$ oxygenate formation over $Cu_{13}$, $Cu_{38}$ and $Cu_{55}$ clusters have been examined, and the most stable adsorption configurations with the adsorption energies on $Cu_{13}$, $Cu_{38}$ and $Cu_{55}$ clusters are presented in Figs. 2–4, respectively.

Our results show that besides $CH_4$ and $C_2H_6$ species, other species are found to be strongly bound to Cu clusters, which is similar to that on the flat and stepped Cu surfaces [65–67]. Table 1 list the adsorption energies and sites of the common species in $C_2$ oxygenate formation on $Cu_{13}$, $Cu_{38}$ and $Cu_{55}$ clusters. For example, the adsorption energies of $CH_2$ species are 412.8, 341.4 and 327.2 kJ $mol^{-1}$ on $Cu_{13}$, $Cu_{38}$ and $Cu_{55}$ clusters, respectively. Obviously, $CH_2$ interaction with $Cu_{13}$ cluster is the strongest, then, $Cu_{38}$ cluster, and $Cu_{55}$ cluster is the weakest.

As shown in Fig. 5, for all common species involved in $C_2$ oxygenate formation on $Cu_{13}$, $Cu_{38}$ and $Cu_{55}$ clusters, the bonding strength of Cu cluster follows the order: $Cu_{13}$ occupies the first place, the second is $Cu_{38}$, $Cu_{55}$ is the third, suggesting that the adsorption ability decreases with the increasing of Cu cluster size. In the view of adsorption configurations, these species are adsorbed at Hcp site on $Cu_{13}$ cluster; at Top I, Bridge I and Hollow sites of (100) facet on $Cu_{38}$ cluster, which is similar to the step edge sites of Cu(211) surface; on $Cu_{55}$ cluster, these species are bonded near the vertex of icosahedron structure, including Top I, Bridge I and Hcp sites.

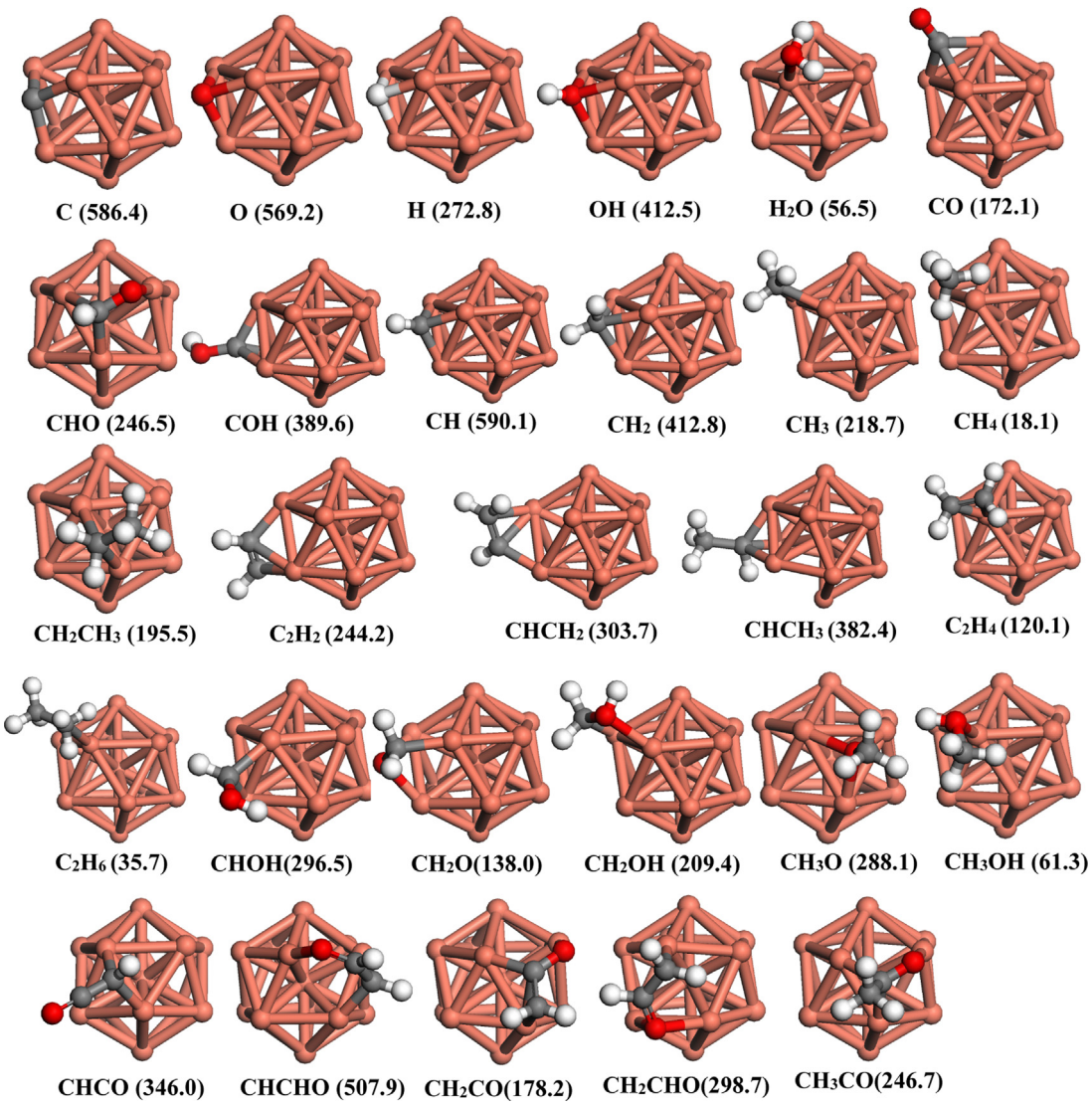


**Fig. 2.** The most stable adsorption configurations of all possible species involved in the formation pathway of $C_2$ oxygenates on $Cu_{13}$ cluster. C, O, H, and Cu atoms are shown in the grey, red, white and orange balls, respectively. The data in the parenthesis are the adsorption energies in kJ $mol^{-1}$. (For interpretation of the references to colour in this figure legend, the reader is referred to the web version of this article.)

**Table 1**
Adsorption sites and adsorption energies ($E_{ads}$/kJ $mol^{-1}$) for the most stable adsorption configurations of the species involved in $C_2$ oxygenates formation from syngas on $Cu_{13}$, $Cu_{38}$ and $Cu_{55}$ clusters.

| Species | $Cu_{13}$ cluster | | $Cu_{38}$ cluster | | $Cu_{55}$ cluster | |
|---|---|---|---|---|---|---|
| | Sites | $E_{ads}$ | Sites | $E_{ads}$ | Sites | $E_{ads}$ |
| C | Hcp | 586.4 | Hollow | 566.5 | Hcp | 509.8 |
| O | Hcp | 569.2 | Hollow | 523.3 | Hcp | 486.5 |
| H | Hcp | 272.8 | Bridge II | 240.3 | Fcc | 239.2 |
| OH | Hcp | 412.5 | Bridge II | 349.3 | Hcp | 302.5 |
| CO | Hcp | 172.1 | Top I | 104.5 | Top I | 109.3 |
| CHO | Hcp | 246.5 | Bridge I | 195.1 | Bridge I | 157.5 |
| COH | Hcp | 389.6 | Hollow | 315.4 | Hcp | 285.4 |
| CH | Hcp | 590.1 | Hollow | 542.5 | Hcp | 485.1 |
| $CH_2$ | Hcp | 412.8 | Hollow | 341.4 | Hcp | 327.2 |
| $CH_3$ | Bridge | 218.7 | Bridge II | 195.7 | Bridge I | 165.1 |
| $CH_4$ | Top | 18.1 | Hcp | 17.2 | Top I | 18.0 |
| CHOH | Bridge | 296.5 | Bridge I | 248.3 | Bridge I | 222.4 |
| $CH_2O$ | Hcp | 138.0 | Hollow | 83.5 | Bridge I | 54.4 |
| $CH_2OH$ | Bridge | 209.4 | Bridge I | 178.7 | Bridge I | 144.7 |
| $CH_3O$ | Hcp | 288.1 | Bridge I | 261.7 | Hcp | 232.3 |
| $CH_3OH$ | Top | 61.3 | Top I | 48.5 | Top I | 49.5 |
| $CH_3CO$ | Hcp | 246.7 | Bridge I | 205.5 | Bridge I | 169.5 |
| $CH_3CHO$ | Hcp | 118.5 | Bridge I | 59.4 | Top I | 65.8 |

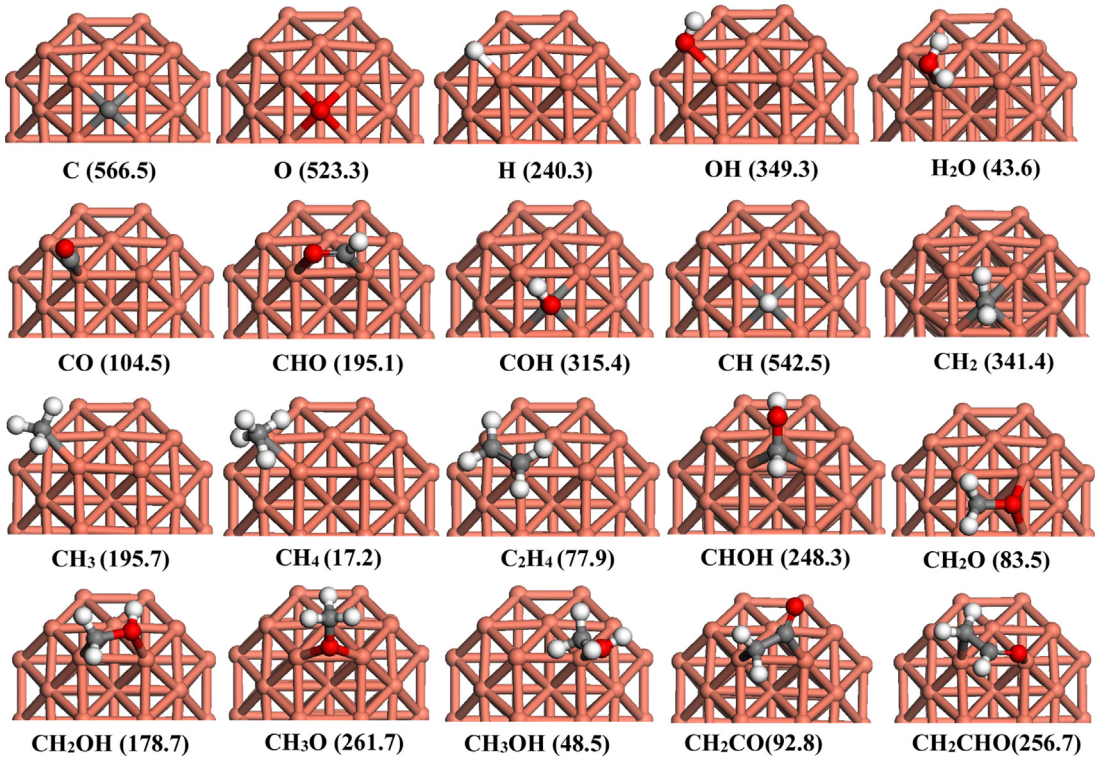


**Fig. 3.** The most stable adsorption configurations and the corresponding adsorption energies of all possible species involved in the formation pathway of $C_2$ oxygenates on $Cu_{38}$ cluster. See Fig. 2 for color coding.

Therefore, it is concluded that the size of Cu cluster obviously affect the adsorption ability of the species involving in $C_2$ oxygenate formation; moreover, the adsorption ability decreases with the increasing of cluster size, which agrees with previous DFT calculations that metal nanoparticles exhibit higher adsorption ability than bulk metal (large particle) [36–38]; among $Cu_{13}$, $Cu_{38}$ and $Cu_{55}$ clusters, $Cu_{13}$ cluster presents the strongest adsorption ability.

### 3.2. $CH_x$(x = 1–3) formation

$CH_x$($x$ = 1–3) formation has two possibilities [67–69]: one is CO direct dissociation into C, followed by C hydrogenation to form $CH_x$($x$ = 1–3); the other is CO hydrogenation to $CH_xO$ or $CH_xOH$ intermediates, followed by its C—O bond cleavage without or with H-assisted to form $CH_x$($x$ = 1–3). Table 2 lists the activation barriers and reaction energies of all possible elementary reactions in $C_2$ oxygenate formation on $Cu_{13}$, $Cu_{38}$ and $Cu_{55}$ clusters. Figs. 6–8 present the potential energy profile for the most favorable formation pathway of $CH_x$($x$ = 1–3) and $CH_3OH$ together with the initial states (ISs), transition states (TSs) and final states (FSs) on $Cu_{13}$, $Cu_{38}$ and $Cu_{55}$ clusters, respectively.

On the other hand, previous studies about CO hydrogenation reactions have not considered the effect of presence of H atom on reaction mechanism [2,70–72], however, the calculated results can clarify the reaction mechanism, which agrees with the reported experiments. Moreover, although a lot of energetically most stable H species exist on the surface in hydrogenation reaction, when the hydrogenation reaction occurs under a realistic condition, only one H adatom interacts with the corresponding adjacent adsorbed species. Thus, the effect of the presence of H atoms on reaction mechanism can be negligible under a realistic condition, as a result, all different hydrogenation steps involve the addition of atomic hydrogen on the surface, and only one H atom is presented on the surface for each hydrogenation step in this study.

#### 3.2.1. CO initial step

Figs. S1–S3 present the potential energy diagram for CO initial step (**R1**–**R3**) together with the ISs, TSs and FSs on $Cu_{13}$, $Cu_{38}$ and $Cu_{55}$ clusters, respectively. Our results show that when CO and H are co-adsorbed on these three Cu clusters, the clusters show rather low catalytic activity toward CO direct dissociation; CO hydrogenation to CHO is more favorable both kinetically and thermodynamically than COH formation and CO direct dissociation.

As a result, CHO is the dominant product of CO initial step on $Cu_{13}$, $Cu_{38}$ and $Cu_{55}$ clusters, which agree with Cu(100), (110), (111) and (211) surfaces [65–67,73]. Thus, we only consider the subsequent formations of $CH_x$, $CH_xO$ and $CH_xOH$ starting with CHO species.

#### 3.2.2. CH formation

Starting from CHO and CHO + H species, the C—O bond cleavage of CHO can form CH (**R4**); CHO hydrogenates to produce CHOH, followed by its C—O bond cleavage to CH (**R5, R6**). Moreover, CHO hydrogenation to $CH_2O$ (**R7**) is examined.

As presented in Figs. S4–S6, on $Cu_{13}$ and $Cu_{55}$ clusters, CH is dominantly formed by the pathway CHO → CH + O (**R4**) with the activation barriers of 139.6 and 206.6 kJ mol$^{-1}$, respectively, which are more favorable than the pathway CHO + H → CHOH → CH + OH (**R5, R6**) with the overall activation barriers of 183.3 and 241.4 kJ mol$^{-1}$, respectively. However, on $Cu_{38}$ cluster, CH is dominantly formed by the pathway CHO + H → CHOH → CH + OH with the overall activation barrier of 193.1 kJ mol$^{-1}$, which is more favorable than the pathway CHO → CH + O with the activation barrier of 261.0 kJ mol$^{-1}$. More importantly, as shown in Figs. 6–8, starting from CHO and CHO + H species, compared to CH formation, CHO + H → $CH_2O$ is the most favorable reaction, which have the much lower activation barriers of 76.5, 76.8 and 64.1 kJ mol$^{-1}$ on $Cu_{13}$, $Cu_{38}$ and $Cu_{55}$ clusters, respectively. Therefore, starting from CHO species, $CH_2O$ is the dominant product on these three Cu clusters.

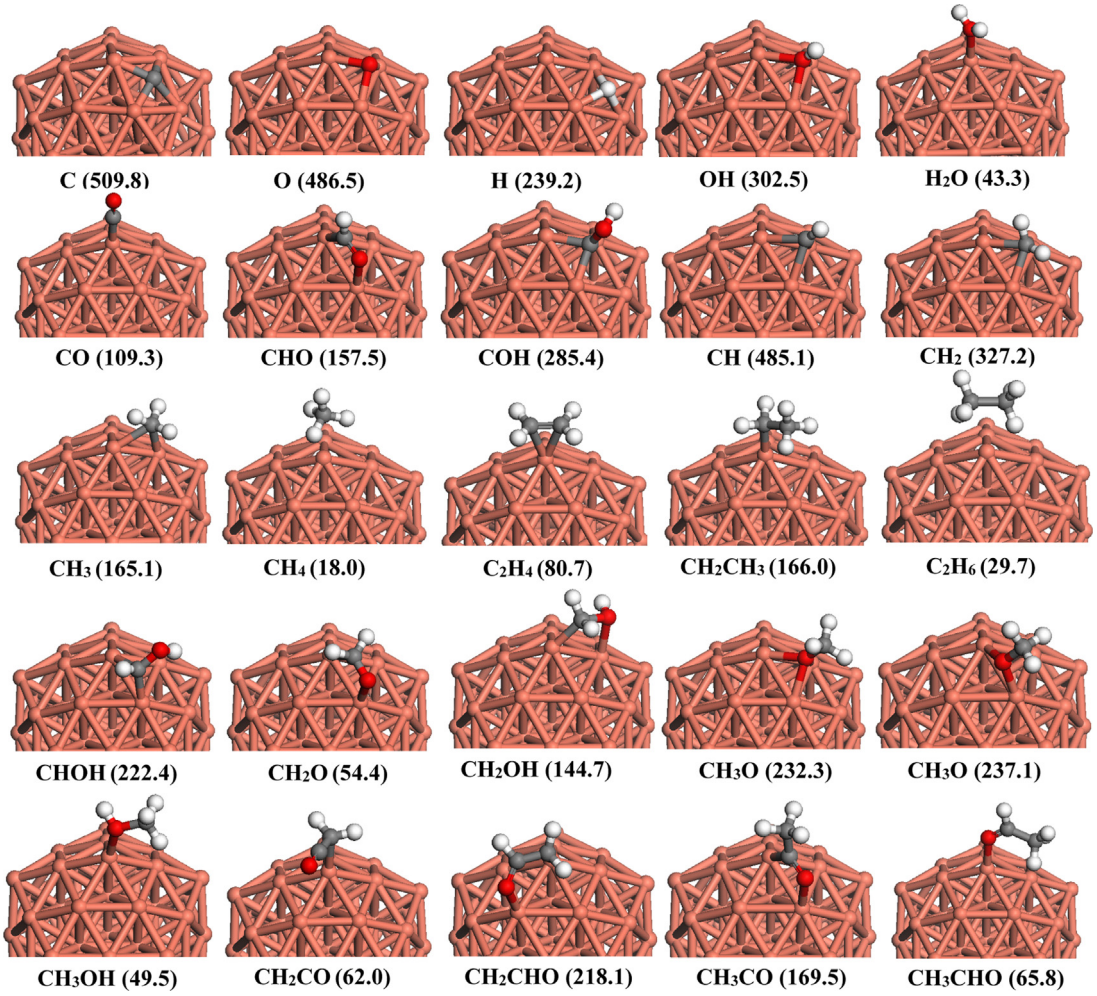


**Fig. 4.** The most stable adsorption configurations and the corresponding adsorption energies of all possible species involved in the formation pathway of $C_2$ oxygenates on $Cu_{55}$ cluster. See Fig. 2 for color coding.

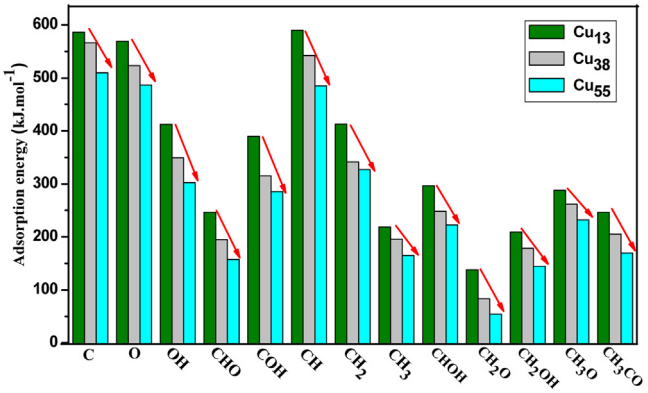


**Fig. 5.** The comparison chart for the adsorption energies of the common species involved in $C_2$ oxygenate formation on $Cu_{13}$, $Cu_{38}$ and $Cu_{55}$ clusters.

### 3.2.3. $CH_2$ formation

Starting from $CH_2O$ species, one is the direct C—O bond cleavage of $CH_2O$ (**R8**) to form $CH_2$; the other is $CH_2O$ hydrogenation to $CH_2OH$ (**R9**), followed by its C—O bond rupture of $CH_2OH$ to form $CH_2$ (**R10**) (see Figs. S7–S9).

As shown in Figs. 6–8, $CH_2$ prefers to be formed by $CH_2O$ direct dissociation ($CH_2O \rightarrow CH_2 + O$) on $Cu_{13}$ cluster; however, $CH_2O + H \rightarrow CH_2OH \rightarrow CH_2 + OH$ is the most favorable pathway of $CH_2$ formation on both $Cu_{38}$ and $Cu_{55}$ clusters. On the other hand, $CH_2O + H \rightarrow CH_3O$ (**R11**) has the lower barrier than $CH_2$ formation, namely, $CH_2O$ prefers to be hydrogenated to $CH_3O$ on these three Cu clusters.

### 3.2.4. $CH_3$ formation

Starting from $CH_3O$ species, the detailed potential energy diagrams of the reactions related to $CH_3$ formation together with the corresponding structures on $Cu_{13}$, $Cu_{38}$ and $Cu_{55}$ clusters are presented in Figs. S10–S12.

Our results show that the pathway $CO + 3H \rightarrow CHO + 2H \rightarrow CH_2O + H \rightarrow CH_3O \rightarrow CH_3 + O$ is dominantly responsible for $CH_3$ formation on three Cu clusters. Moreover, $CH_3O$ hydrogenation to $CH_3OH$ (**R14**) is considered. By comparison, $CH_3$ formation is more favorable $CH_3OH$ formation on $Cu_{13}$ cluster; however, $CH_3O$ prefers to be hydrogenated to $CH_3OH$ rather than being formed $CH_3$ in kinetics on both $Cu_{38}$ and $Cu_{55}$ clusters.

### 3.2.5. The most favorable $CH_x$ ($x = 1–3$) monomer and $CH_3OH$ formations

On $Cu_{13}$ cluster, as shown in Fig. 6, with respect to CO + H species, CH is formed via the pathway of $CO + H \rightarrow CHO \rightarrow CH + O$ with the overall barrier and reaction energy of 225.5 and 190.0 kJ mol$^{-1}$; $CH_2$ is formed via the pathway of $CO + 2H \rightarrow CHO + H \rightarrow CH_2O \rightarrow CH_2 + O$ with the overall barrier and reaction energy of 226.9 and 42.6 kJ mol$^{-1}$; $CH_3$ is formed via

**Table 2**
Calculated activation barriers ($E_a$/kJ mol$^{-1}$) and reaction energies ($\Delta H$/kJ mol$^{-1}$) of the elementary reactions involved in $C_2$ oxygenates from syngas on $Cu_{13}$, $Cu_{38}$ and $Cu_{55}$ clusters.

| Elementary reactions | | $Cu_{13}$ cluster | | $Cu_{38}$ cluster | | $Cu_{55}$ cluster | |
|---|---|---|---|---|---|---|---|
| | | $E_a$ | $\Delta H$ | $E_a$ | $\Delta H$ | $E_a$ | $\Delta H$ |
| (R1) | CO → C + O | 361.3 | 199.0 | 332.7 | 140.7 | 371.8 | 213.6 |
| (R2) | CO + H → CHO | 139.3 | 85.9 | 108.0 | 53.8 | 163.7 | 82.4 |
| (R3) | CO + H → COH | 313.6 | 136.6 | 305.4 | 106.9 | 328.5 | 133.3 |
| (R4) | CHO → CH + O | 139.6 | 104.1 | 261.0 | 14.6 | 206.6 | 55.4 |
| (R5) | CHO + H → CHOH | 145.8 | 96.7 | 157.5 | 52.9 | 110.9 | 51.5 |
| (R6) | CHOH → CH + OH | 86.6 | −82.0 | 140.2 | −106.4 | 189.9 | −34.8 |
| (R7) | CHO + H → $CH_2O$ | 76.5 | 5.0 | 76.8 | −20.7 | 64.1 | −15.0 |
| (R8) | $CH_2O$ → $CH_2$ + O | 136.0 | −48.3 | 215.1 | 9.0 | 246.2 | 43.2 |
| (R9) | $CH_2O$ + H → $CH_2OH$ | 158.5 | 74.2 | 150.0 | 27.3 | 106.6 | 5.3 |
| (R10) | $CH_2OH$ → $CH_2$ + OH | 90.0 | −104.0 | 110.0 | −50.8 | 132.4 | −29.9 |
| (R11) | $CH_2O$ + H → $CH_3O$ | 106.6 | −22.8 | 65.7 | −39.1 | 38.6 | −64.1 |
| (R12) | $CH_3O$ → $CH_3$ + O | 155.0 | −71.0 | 210.7 | −25.2 | 201.9 | −26.3 |
| (R13) | $CH_3O$ + H → $CH_3$ + OH | – | – | – | – | 271.8 | −23.4 |
| (R14) | $CH_3O$ + H → $CH_3OH$ | 208.5 | 87.6 | 188.6 | 48.4 | 177.1 | 11.8 |
| (R15) | CH + CO → CHCO | 90.1 | −7.7 | – | – | – | – |
| (R16) | CH + CHO → CHCHO | 76.9 | −108.9 | – | – | – | – |
| (R17) | CH + H → $CH_2$ | 102.4 | 7.8 | – | – | – | – |
| (R18) | CH → C + H | 182.9 | 72.3 | – | – | – | – |
| (R19) | CH + CH → $C_2H_2$ | 91.3 | −117.2 | – | – | – | – |
| (R20) | CH + $CH_2$ → $CHCH_2$ | 169.6 | −41.3 | – | – | – | – |
| (R21) | CH + $CH_3$ → $CHCH_3$ | 98.0 | −1.2 | – | – | – | – |
| (R22) | $CH_2$ + CO → $CH_2CO$ | 208.4 | 5.8 | 86.0 | −19.5 | 191.1 | −11.1 |
| (R23) | $CH_2$ + CHO → $CH_2CHO$ | 160.1 | −84.3 | 99.8 | −149.7 | 131.2 | −142.7 |
| (R24) | $CH_2$ + H → $CH_3$ | 141.8 | 7.3 | 99.1 | −54.2 | 111.1 | 41.9 |
| (R25) | $CH_2$ → CH + H | 94.5 | −7.8 | 95.3 | −25.2 | 174.4 | 34.2 |
| (R26) | $CH_2$ + $CH_2$ → $C_2H_4$ | 240.2 | −29.8 | 160.4 | −138.8 | 194.8 | −130.9 |
| (R27) | $CH_2$ + $CH_3$ → $CH_2CH_3$ | 160.4 | 12.8 | – | – | 174.1 | −54.4 |
| (R28) | $CH_3$ + CO → $CH_3CO$ | 137.4 | 29.6 | – | – | 129.3 | 1.5 |
| (R29) | $CH_3$ + CHO → $CH_3CHO$ | 66.2 | −29.9 | – | – | 90.4 | −100.3 |
| (R30) | $CH_3$ + H → $CH_4$ | 147.9 | 32.3 | 162.1 | −23.9 | 106.3 | −47.6 |
| (R31) | $CH_3$ → $CH_2$ + H | 149.0 | 7.3 | – | – | 162.5 | 51.3 |
| (R32) | $CH_3$ + $CH_3$ → $C_2H_6$ | 199.5 | 34.7 | – | – | 180.9 | −77.3 |
| (R33) | CHCO + H → $CH_2CO$ | 170.4 | 16.3 | – | – | – | – |
| (R34) | CHCO + H → CHCHO | 121.4 | −19.8 | – | – | – | – |
| (R35) | CHCO + H → CHCOH | 224.6 | 64.5 | – | – | – | – |
| (R36) | CHCHO + H → $CH_2CHO$ | 134.7 | −3.3 | – | – | – | – |
| (R37) | CHCHO + H → CHCHOH | 161.0 | 100.5 | – | – | – | – |

the pathway of CO + 3H → CHO + 2H → $CH_2O$ + H → $CH_3O$ → $CH_3$ + O with the overall barrier and reaction energy of 223.1 and −2.9 kJ mol$^{-1}$; $CH_3OH$ is formed via the pathway of CO + 4H → CHO + 3H → $CH_2O$ + 2H → $CH_3O$ + H → $CH_3OH$ with the overall barrier and reaction energy of 276.6 and 155.7 kJ mol$^{-1}$. These results show that $CH_x$ ($x$ = 1–3) formations have the similar overall barrier, which are much lower than $CH_3OH$ formation (225.5/226.9/223.1 *vs.* 276.6 kJ mol$^{-1}$). As a result, all $CH_x$ ($x$ = 1–3) species are abundant on $Cu_{13}$ cluster rather than $CH_3OH$, namely, the small $Cu_{13}$ cluster exhibits the high selectivity toward $CH_x$ ($x$ = 1–3) rather than $CH_3OH$.

On $Cu_{38}$ cluster, as shown in Fig. 7, with respect to CO + H species, the overall barrier of $CH_2$ formation (CO + H → CHO + H → $CH_2O$ + H → $CH_2OH$ → $CH_2$ + OH) is lower than CH and $CH_3$ formations (183.1 *vs.* 211.3/204.7 kJ mol$^{-1}$), indicating that $CH_2$ is the most favored $CH_x$ monomer. For $CH_3OH$ formation, the most favorable route is CO + 4H → CHO + 3H → $CH_2O$ + 2H → $CH_3O$ + H → $CH_3OH$ with the overall barrier of 182.6 kJ mol$^{-1}$, which is energetically compatible with the formation of the most favored $CH_2$ monomer (183.1 kJ mol$^{-1}$).

On $Cu_{55}$ cluster, as shown in Fig. 8, with respect to CO + H species, CH, $CH_2$ and $CH_3$ formations (CO + H → CHO → CH + O, CO + 3H → CHO + 2H → $CH_2O$ + H → $CH_2OH$ → $CH_2$ + OH and CO + 3H → CHO + 2H → $CH_2O$ + H → $CH_3O$ → $CH_3$ + O) have the overall barriers of 289.0, 205.1 and 205.2 kJ mol$^{-1}$, respectively, which are less favorable than $CH_3OH$ formation (CO + 4H→ CHO + 3H → $CH_2O$ + 2H → $CH_3O$ + H → $CH_3OH$) with the overall barrier of 180.4 kJ mol$^{-1}$. Thus, both $CH_2$ and $CH_3$ species are the most favored $CH_x$ monomer; however, $CH_3OH$ is the main product on $Cu_{55}$ cluster.

On the basis of above results, we can conclude that $CH_x$ ($x$ = 1–3) species are abundant on $Cu_{13}$ cluster rather than $CH_3OH$. On $Cu_{38}$ cluster, only $CH_2$ monomer is the abundant $CH_x$ species, which competes with $CH_3OH$ formation. However, on $Cu_{55}$ clusters, $CH_3OH$ formation is more favorable than the most favored monomer $CH_2$ and $CH_3$ species. Thus, compared to $CH_3OH$ formation, the selectivity of $CH_x$($x$ = 1–3) species decreases with the increasing of Cu cluster size. As a result, $Cu_{13}$ cluster can provide more abundant $CH_x$ species to participate into $C_2$ species formation than other larger Cu clusters, moreover, more $CH_x$ sources are beneficial to produce $C_2$ oxygenates [2,65,68,74].

### 3.3. C—C chain formation of $C_2$ oxygenates

For C—C chain formation, previous studies by Zhao et al. [75] found that CHO insertion into $CH_x$ ($x$ = 1–3) is superior and/or competitive to CO insertion and carbene coupling on Rh(111) and Co(0001) surface; moreover, Wang et al. [65,66] have shown that both $CH_2$ and $CH_3$ species are the precursor for C—C chain formation on Cu(110) and Cu(100) surfaces.

In this section, we further investigate CO/CHO insertion into the most favored $CH_x$ monomer to form $C_2$ oxygenates, and $CH_x$ coupling to form $C_2$ hydrocarbons, as well as $CH_x$ dissociation and hydrogenation on $Cu_{13}$, $Cu_{38}$ and $Cu_{55}$ clusters, respectively. Fig. 9 presents the simplified potential energy profile for the most

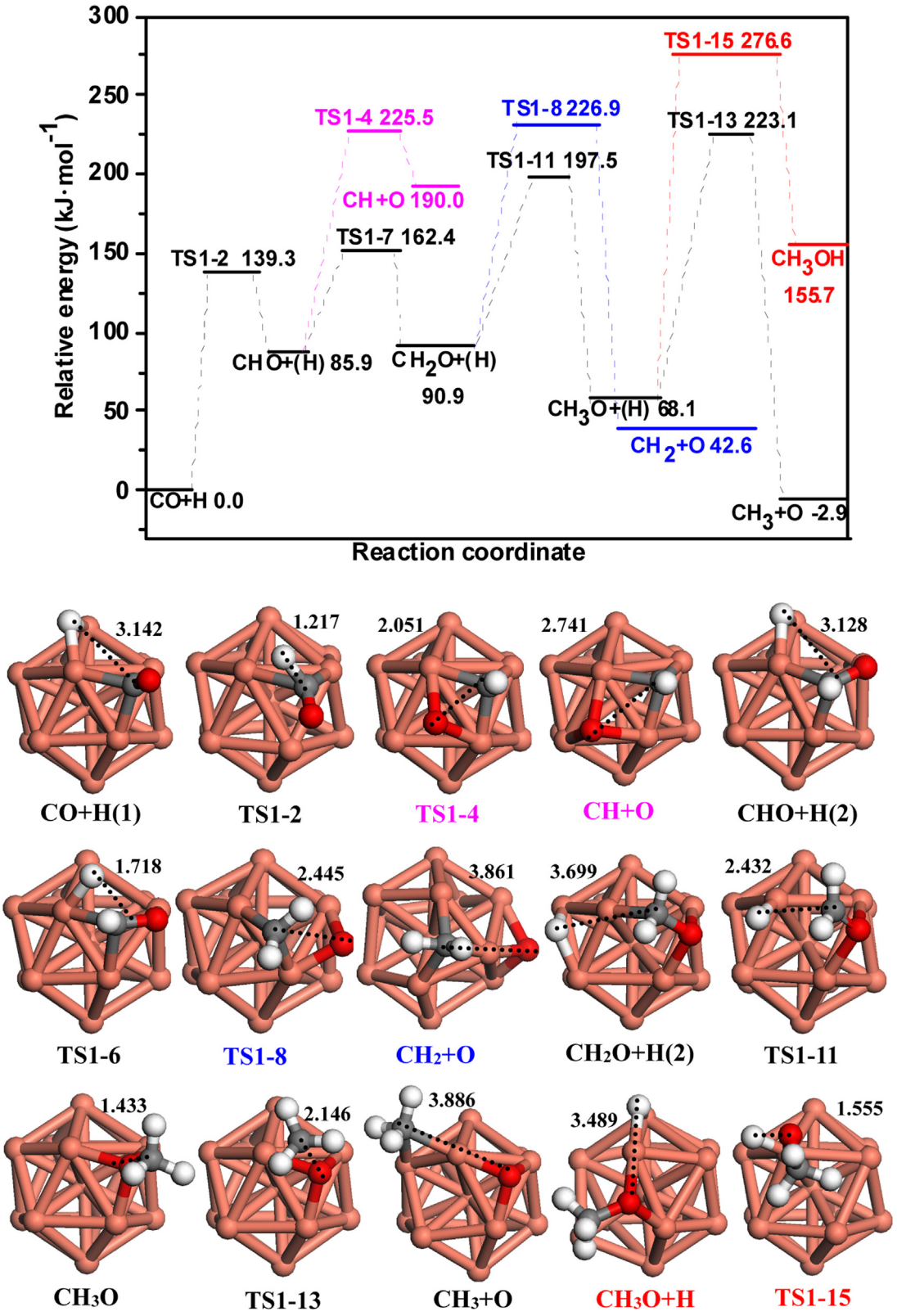


**Fig. 6.** The potential energy diagram of the most favorable formation pathway for $CH_x$($x$ = 1-3) species and $CH_3OH$ together with the initial states (ISs), transition states (TSs) and final states (FSs) on $Cu_{13}$ cluster. Bond lengths are in Å. See Fig. 2 for color coding.

favorable pathway of $C_2$ oxygenates formation on $Cu_{13}$, $Cu_{38}$ and $Cu_{55}$ clusters.

### 3.3.1. $Cu_{13}$ cluster

Since $CH_x$($x$ = 1–3) species are abundant on $Cu_{13}$ cluster rather than $CH_3OH$, all reactions related to $CH_x$($x$ = 1–3) species are examined on $Cu_{13}$ cluster.

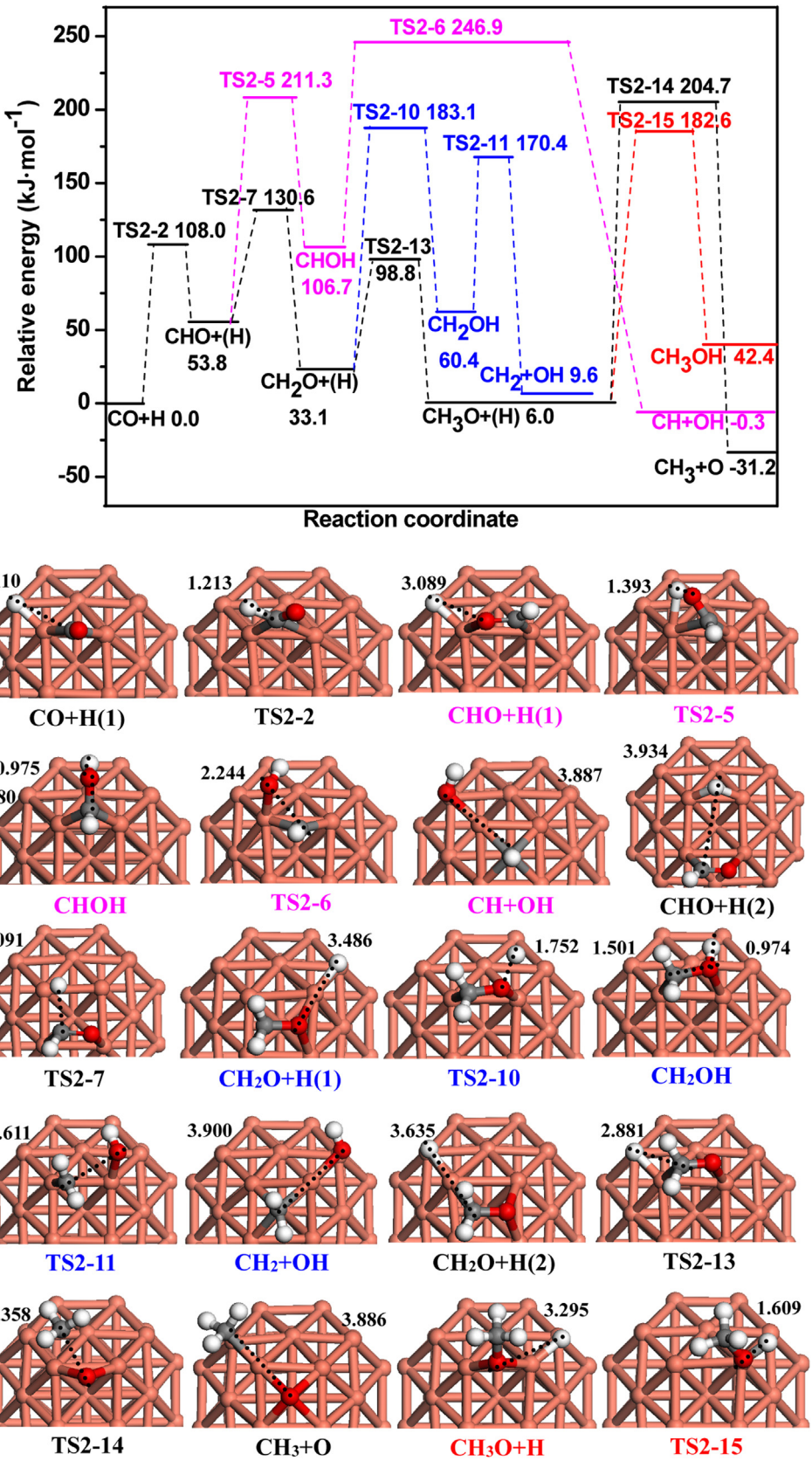


**Fig. 7.** The potential energy diagram of the most favorable formation pathway for $CH_x$($x$ = 1–3) species and $CH_3OH$ together with the ISs, TSs and FSs on $Cu_{38}$ cluster. Bond lengths are in Å. See Fig. 2 for color coding.

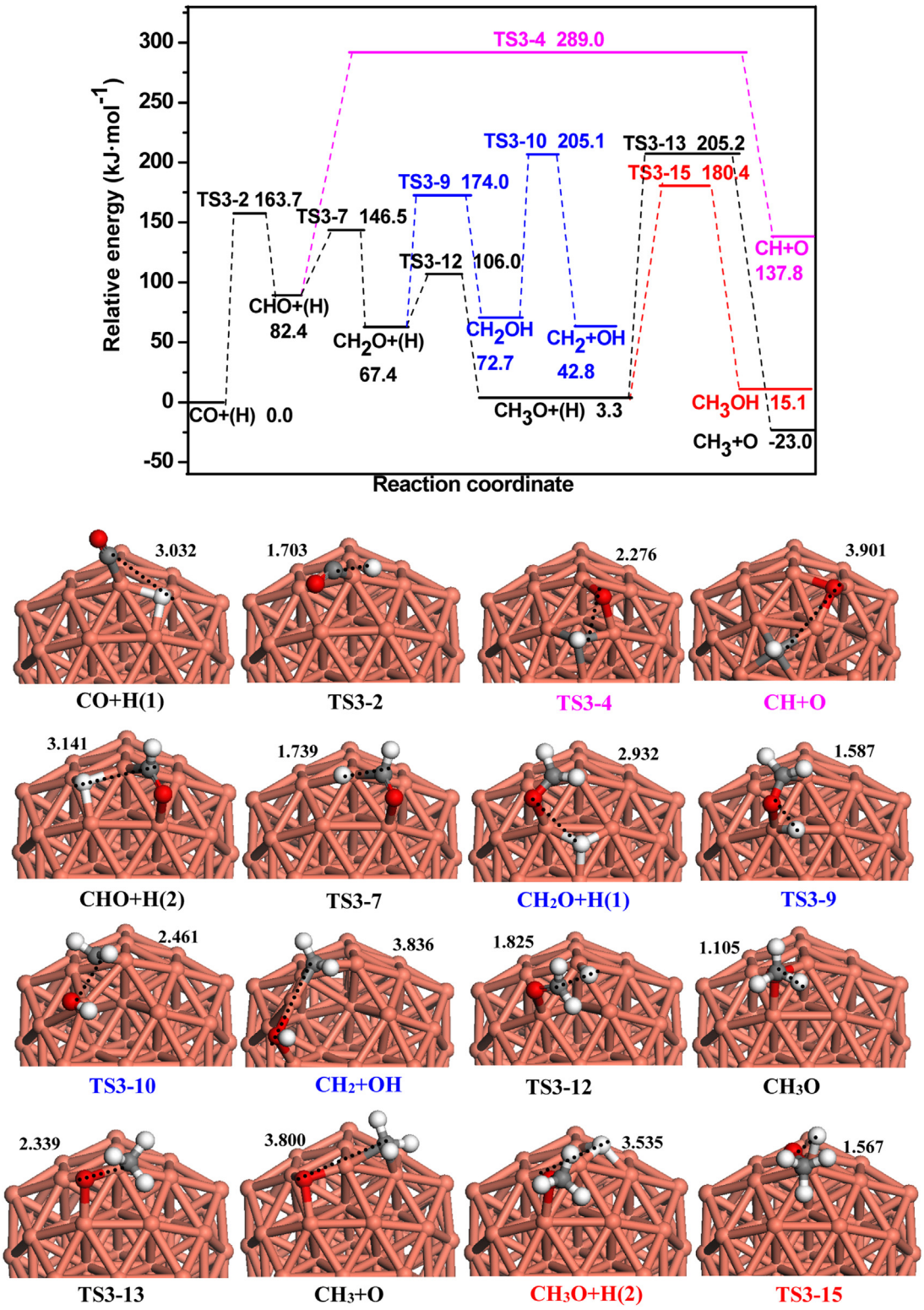


**Fig. 8.** The potential energy diagram of the most favorable formation pathway for $CH_x$ ($x$ = 1–3) species and $CH_3OH$ together with the ISs, TSs and FSs on $Cu_{55}$ cluster. Bond lengths are in Å. See Fig. 2 for color coding.

As shown in Fig. S13, for CH species, considering CHO formation by CO hydrogenation, it can be found that CH species prefers to form $C_2$ oxygenate CHCO by CO insertion into CH (CH + CO → CHCO) rather than that by CHO insertion (90.1 *vs.* 162.8 kJ mol$^{-1}$). Moreover, among all reactions related to CH species (**R15–R21**), only the reaction of CH + CH → $C_2H_2$ is competitive with CO insertion (91.3 *vs.* 90.1 kJ mol$^{-1}$). However, CO is the most abundant species in syngas conversion confirmed by experiment [76], the coverage of CO reaches 0.5 ML on Cu(100) surface [77] and Co(0001) surface [78] under the realistic conditions. Therefore, CO insertion into CH can be accelerated by the abundant coverage of CO; namely,

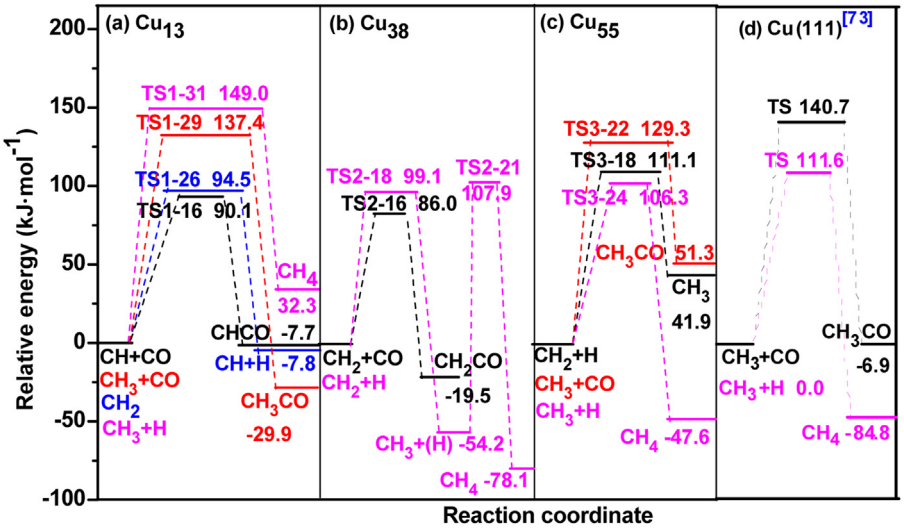


**Fig. 9.** The comparison of the simplified potential energy profile for the most favorable formation pathways of $C_2$ oxygenates and $CH_4$ on (a) $Cu_{13}$, (b) $Cu_{38}$, (c) $Cu_{55}$ clusters, and (d) Cu(111) surface.

$C_2$ oxygenate CHCO is the major product from CH species rather than $C_2$ hydrocarbon $C_2H_2$.

As shown in Fig. S14, for $CH_2$ species, $CH_2$ dissociation into CH is the most favorable reaction with the activation barrier and reaction energy of 94.5 and −7.8 kJ mol$^{-1}$ among all reactions related to $CH_2$ species (**R22**–**R27**); subsequently, once CH species is formed, CO insertion into CH species leads to $C_2$ oxygenate CHCO. Thus, $C_2$ oxygenates CHCO is the major product from $CH_2$ species.

As shown in Fig. S17, for $CH_3$ species, $CH + CH_3 \rightarrow CHCH_3$ is the most favorable pathway with the lowest activation barrier of 98.0 kJ mol$^{-1}$; Secondly, CO insertion into $CH_3$ to $CH_3CO$ has the activation barrier of 137.4 kJ mol$^{-1}$; Thirdly, $CH_3$ hydrogenation to $CH_4$ has the activation barrier of 147.9 kJ mol$^{-1}$. However, CH species prefers to interact with CO to form CHCO with the activation barrier of 90.1 kJ mol$^{-1}$ rather than CH coupling with $CH_3$ to $CH_3CH$, moreover, similar to CH species, due to the abundant coverage of CO, CO prefers to insert into $CH_3$ to form $CH_3CO$. Thus, $C_2$ oxygenate $CH_3CO$ is the main product from $CH_3$ species on $Cu_{13}$ cluster.

On the basis of above results, we can obtain that the abundant $CH_x$($x$ = 1–3) species on $Cu_{13}$ cluster dominantly contribute to the formation of $C_2$ oxygenates CHCO and $CH_3CO$.

### 3.3.2. $Cu_{38}$ cluster

$CH_2$ species is the most favored $CH_x$ monomer on $Cu_{38}$ cluster, as shown in Fig. S15, among all reactions related to $CH_2$ species (**R22**–**R26**), CO insertion into $CH_2$ to $CH_2CO$ is the most favorable reaction, which has the activation barrier and reaction energy of 88.9 and −26.6 kJ mol$^{-1}$, respectively. Thus, the abundant $CH_2$ species on $Cu_{38}$ cluster dominantly contribute to the formation of $C_2$ oxygenate $CH_2CO$. In addition, $CH_4$ formation by $CH_3$ hydrogenation is also examined, this elementary reaction has an activation barrier of 162.1 kJ mol$^{-1}$, and it is exothermic by 23.9 kJ mol$^{-1}$.

### 3.3.3. $Cu_{55}$ cluster

Both $CH_2$ and $CH_3$ species are the most favored $CH_x$ monomer, as shown in Fig. S16, for $CH_2$ species, $CH_2 + H \rightarrow CH_3$ is the most favorable reaction, which has the activation barrier and reaction energy of 111.1 and 41.9 kJ mol$^{-1}$, respectively. Secondly, $CH_3$ coupling with $CH_2$ to $CH_3CH_2$ has a significantly high activation barrier of 174.1 kJ mol$^{-1}$ with reaction energy of −54.4 kJ mol$^{-1}$. As shown below, once $CH_3$ is formed by $CH_2$ hydrogenation, $CH_3$ prefers to be hydrogenated to form $CH_4$. Thus, $CH_4$ is the major product from $CH_2$ species.

As shown in Fig. S18, for $CH_3$ species, $CH_3$ prefers to be hydrogenated to $CH_4$ with the activation barrier and reaction energy of 106.3 and −47.6 kJ mol$^{-1}$, respectively; Secondly, CO insertion into $CH_3$ to $C_2$ oxygenates $CH_3CO$ has the activation barrier and reaction energy of 129.3 and 1.5 kJ mol$^{-1}$, respectively. Thus, $CH_4$ is the major product from $CH_3$ species.

On the basis of above results, on $Cu_{55}$ cluster, $C_2$ oxygenates $CH_3CO$ is dominantly formed by CO insertion into $CH_3$, however, $CH_3$ hydrogenation to $CH_4$ is more favorable than CO insertion (106.3 *vs.* 129.3 kJ mol$^{-1}$), in which $CH_3$ species has two sources: one is $CH_3O$ direct dissociation, the other is $CH_2$ hydrogenation. As a result, the abundant $CH_2$ and $CH_3$ species on $Cu_{55}$ cluster dominantly contribute to $CH_4$ formation.

## 3.4. Ethanol formation

As mentioned above, $C_2$ oxygenate is dominantly formed by CO insertion into $CH_x$. Both CHCO and $CH_3CO$ are the dominant $C_2$ oxygenates on $Cu_{13}$ cluster; $CH_2CO$ and $CH_3CO$ are the dominant $C_2$ oxygenates on $Cu_{38}$ and $Cu_{55}$ clusters, respectively. In this section, ethanol formation by the successive hydrogenations of $CH_xCO$(x = 1–3) has been examined on three Cu clusters, as shown in Figs. S19–S22.

On $Cu_{13}$ cluster, starting from CHCO and $CH_3CO$, ethanol is formed by the pathway $CHCO + 5H \rightarrow CHCHO + 4H \rightarrow CH_2CHO + 3H \rightarrow CH_3CHO + 2H \rightarrow CH_3CH_2O + H \rightarrow C_2H_5OH$ and $CH_3CO + 3H \rightarrow CH_3CHO + 2H \rightarrow CH_3CH_2O + H \rightarrow C_2H_5OH$, respectively. Whereas, starting from $CH_3CO$, the pathway is $CH_3CO + 3H \rightarrow CH_3COH + 2H \rightarrow CH_3CHOH + H \rightarrow C_2H_5OH$ on $Cu_{55}$ cluster. However, on $Cu_{38}$ cluster, starting from $CH_2CO$, the pathway is $CH_2CO + 4H \rightarrow CH_2CHO + 3H \rightarrow CH_3CHO + 2H \rightarrow CH_3CH_2O + H \rightarrow C_2H_5OH$.

## 3.5. General discussion

### 3.5.1. The active sites of $Cu_{13}$, $Cu_{38}$ and $Cu_{55}$ clusters

On the basis of above DFT calculations, the adsorption energy of the species in $C_2$ oxygenate formation is significantly influenced by the size of Cu cluster. Most of species are adsorbed at Hcp site on $Cu_{13}$ cluster; the species on $Cu_{38}$ cluster are positioned at (100) facet, including Top I, Bridge I and Hollow sites; the species on $Cu_{55}$

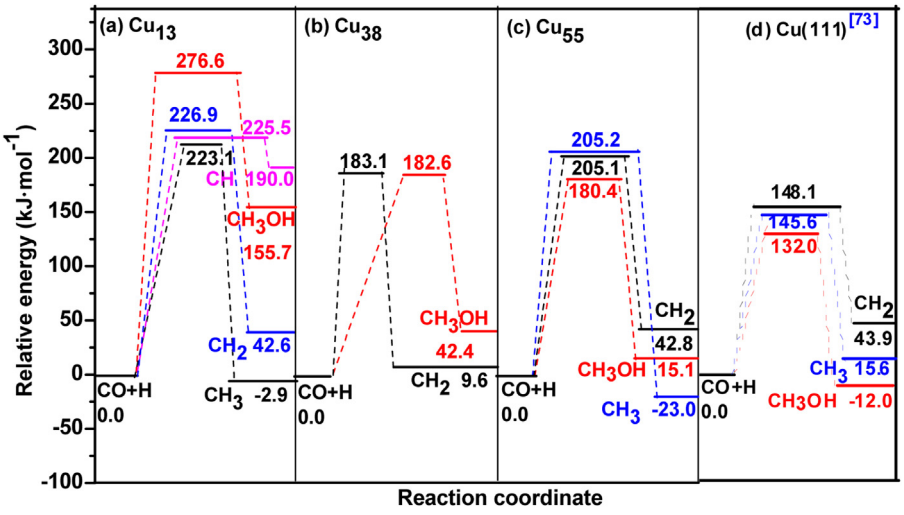


**Fig. 10.** The comparison of the simplified potential energy profile for the most favorable formation pathways of $CH_x$($x$ = 1–3) and $CH_3OH$ on (a) $Cu_{13}$, (b) $Cu_{38}$, (c) $Cu_{55}$ clusters, and (d) Cu(111) surface.

cluster are located near the vertex of the icosahedron, including Top I, Bridge I and Hcp sites. Interestingly, these favorable adsorption sites are all edge sites on three Cu clusters, which are similar to the stepped surfaces, suggesting that the edge sites exhibit the higher activity than other adsorption sites.

The high activity of edge sites corresponds to the low coordination number, which can lead to high energy of *d*-band center. Wherein, for $Cu_{13}$ cluster, all shell atoms have only 6 coordination atoms, which exhibit the strongest adsorption ability, $Cu_{55}$ cluster is the most poor, namely, the adsorption ability decreases with the increasing of cluster size. Moreover, most of the elementary reactions involved in $C_2$ oxygenate formation also occurs at the edge sites of Cu clusters. Further, the enhanced adsorption ability of the adsorbed species, especially for $CH_x$($x$ = 1–3), C, O and OH, at $Cu_{13}$ cluster with the low coordination number becomes a thermodynamic driving force to lower the barrier for C—O bond breaking reaction [75,76].

### 3.5.2. *The effect of Cu cluster size on the selectivity between $CH_x$ and $CH_3OH$*

According to our calculated results, CHO species is the major product of CO initial step on $Cu_{13}$, $Cu_{38}$ and $Cu_{55}$ clusters, which agrees with the previous studies on the flat and stepped Cu periodic surfaces [65–67,73]. Since $CH_3OH$ is easily formed from syngas on Cu catalyst, which affects the productivity and selectivity of $CH_x$ species, our results show that $CO + 4H \rightarrow CHO + 3H \rightarrow CH_2O + 2H \rightarrow CH_3O + H \rightarrow CH_3OH$ is the favorable pathway of $CH_3OH$ formation on three Cu clusters, namely, the effect of Cu cluster size on $CH_3OH$ formation pathway is negligible, which agrees well with the previous reported results [65–67,76,79–81].

For $CH_x$ formation, as shown in Fig. 10, $CH_x$($x$ = 1–3) species are abundant on $Cu_{13}$ cluster; only $CH_2$ is abundant on $Cu_{38}$ cluster; both $CH_2$ and $CH_3$ species are the abundant on $Cu_{55}$ cluster and Cu(111) surface [73]; Thus, $CH_2$ is always the abundant $CH_x$ species on $Cu_{13}$, $Cu_{38}$ and $Cu_{55}$ clusters, as well as Cu(111) surface.

In order to better understand the effect of Cu cluster size on the selectivity of $CH_x$ species in syngas conversion, it is necessary to quantify the selectivity between the most favored $CH_x$ monomer and $CH_3OH$ on $Cu_{13}$, $Cu_{38}$ and $Cu_{55}$ clusters, which is determined by the effective barrier difference between $CH_x$ and $CH_3OH$ [82]. In general, the higher barrier differences between $CH_x$ and $CH_3OH$ represent the higher selectivity of $CH_x$. As shown in Fig. 10, the overall barrier differences between the most favored $CH_x$ monomer and $CH_3OH$ are 51.1, 49.7 and 53.5 kJ mol$^{-1}$ on $Cu_{13}$ cluster, −0.5 kJ mol$^{-1}$ on $Cu_{38}$ cluster, −24.8 and −24.7 kJ mol$^{-1}$ on $Cu_{55}$ cluster, as well as −13.6 and −16.1 kJ mol$^{-1}$ on Cu(111) surface [73], respectively, suggesting that $CH_x$ formation is more favorable kinetically than $CH_3OH$ formation on $Cu_{13}$ cluster, namely, $Cu_{13}$ cluster exhibits a good selectivity toward $CH_x$($x$ = 1–3) species rather than $CH_3OH$. On $Cu_{38}$ cluster, the most favored $CH_2$ monomer competes with $CH_3OH$ formation, which reduces the productivity and selectivity of $CH_2$. However, on $Cu_{55}$ cluster, $CH_3OH$ prefers to be produced rather than $CH_x$($x$ = 1–3) species, which is similar to Cu(111) surface [73], suggesting that the size of $Cu_{55}$ cluster has presented a similar catalytic performance with Cu bulk surface.

On the basis of above analysis, we can conclude that the selectivity of $CH_x$($x$ = 1–3) species formed by syngas decreases with the increasing of Cu cluster size. Therefore, $Cu_{13}$ cluster may exhibits a good selectivity toward $CH_x$($x$ = 1–3) species rather than $CH_3OH$ compared to other large Cu clusters, which can be attributed to that the enhanced adsorption ability of the adsorbed species, especially for $CH_x$($x$ = 1–3), C, O and OH at $Cu_{13}$ cluster, becomes a thermodynamic driving force to lower the barrier for C—O bond breaking reaction [75,76]. As a matter of fact, when the more concentration of $CH_x$ monomer can be obtained to participate into the C—C chain formation, the productivity and selectivity of $C_2$ species may be significantly improved.

### 3.5.3. *The effect of Cu cluster size between $C_2$ oxygenates and $CH_4$*

As shown in Section 3.3, t on $Cu_{13}$ cluster, starting from the most favored $CH_x$($x$ = 1–3) species, $C_2$ oxygenates CHCO and $CH_3CO$ are the dominant products of $C_2$ species. On $Cu_{38}$ cluster, starting from $CH_2$ species, $C_2$ oxygenate $CH_2CO$ is the dominant product of $C_2$ species. On $Cu_{55}$ cluster, starting from $CH_2$ and $CH_3$ species, $C_2$ oxygenate $CH_3CO$ is the dominant product of $C_2$ species. However, along with $C_2$ oxygenate formation, $CH_x$ species can be also hydrogenated to form $CH_4$, which can affect the productivity and selectivity of $C_2$ oxygenates.

As shown in Fig. 9, on $Cu_{13}$ cluster, the overall barrier differences between CHCO/$CH_3CO$ and $CH_4$ formation are 58.9 and 11.6 kJ mol$^{-1}$. On $Cu_{38}$ cluster, the value between $CH_2CO$ and $CH_4$ is 21.9 kJ mol$^{-1}$. On $Cu_{55}$ cluster, the values between $CH_3CO$ and $CH_4$ is −23.0 kJ mol$^{-1}$. On Cu(111) surface, the values is −29.1 kJ mol$^{-1}$. It can be found that once $CH_x$ ($x$ = 1–3) monomer is formed,

$C_2$ oxygenates are always the dominant products on both $Cu_{13}$ and $Cu_{38}$ clusters. However, on $Cu_{55}$ cluster and Cu(111) surface, $CH_4$ formation is more preferable than $C_2$ oxygenates, namely, the catalytic performance of $Cu_{55}$ cluster is similar to Cu bulk surface. Therefore, the selectivity of $C_2$ oxygenates on Cu catalyst decreases with the increasing of Cu cluster size.

Above comparisons about Cu cluster size show that on $Cu_{13}$ cluster, the productivity and selectivity of $C_2$ oxygenates is higher than other cluster size, and Cu cluster size can affect the selectivity toward $C_2$ oxygenates; moreover, the smaller Cu cluster size is, the higher the selectivity of $C_2$ oxygenates is. That is probably related to the high concentration of low-coordinated defect sites on small size Cu cluster, which results in the higher activity and selectivity toward $C_2$ oxygenates.

#### 3.5.4. Implications for $C_2$ oxygenate formation from syngas on Cu catalyst

Above results clearly demonstrate that Cu cluster size can induce significant changes to the adsorption energies, and therefore to the thermodynamics and kinetics of elementary processes. Among $Cu_{13}$, $Cu_{38}$, $Cu_{55}$ clusters, on $Cu_{13}$ cluster, the formations of $CH_x$ and $C_2$ oxygenates are more favorable than $CH_3OH$ and $CH_4$, suggesting that $Cu_{13}$ cluster exhibit the highest catalytic selectivity toward $C_2$ oxygenates rather than $CH_3OH$ and $CH_4$. On $Cu_{38}$ cluster, $CH_x$ formation competes with $CH_3OH$, $C_2$ oxygenate formation is favorable than $CH_4$ formation, namely, $Cu_{38}$ cluster presents the high selectivity toward $C_2$ oxygenates and $CH_3OH$ formations. On $Cu_{55}$ cluster and the periodic Cu(111) surface, $CH_3OH$ formation is more favorable than $CH_x$ formation, which leads to less $CH_x$ sources to participate into $C_2$ oxygenates and $CH_4$ formations, namely, $Cu_{55}$ cluster and the periodic Cu(111) surface presents the high selectivity toward $CH_3OH$ formation.

The identification of higher intrinsic selectivity of $C_2$ oxygenates, active sites, and stronger cluster size effect of Cu catalyst would be valuable for developing more efficient and stable Cu catalysts with higher selectivity toward $C_2$ oxygenates in syngas conversion. Since the selectivity of $C_2$ oxygenates on Cu catalyst decreases with the increasing of Cu cluster size, we could resort to cluster size control by preparing a large number of small size Cu cluster, such as, $Cu_{13}$ cluster, to increase the selectivity of Cu catalyst toward $C_2$ oxygenates. Due to the progress of material synthesis, it would be highly valuable to synthesize $Cu_{13}$ cluster.

The understanding about the effect of Cu cluster size in tuning catalytic performance at the atomic level can potentially be used to develop and design improved catalysts for $C_2$ oxygenate synthesis and other important reactions of interest, in which DFT calculations and material synthesis would play an essential role. In addition, under the realistic conditions of syngas conversion, the presences of support and promoter for the catalysts may have a significant effect on the binding of adsorbed species, even for the preferred reaction paths; this study only focus the discussion on the effect of cluster size on two crucial competing processes, $CH_x$ and $C_2$ oxygenate formations. Qualitative investigations into the effects of support and promoter with extensive theoretical calculations would be desirable in our future work.

## 4. Conclusions

A comparative study about the formation mechanism of $CH_x(x = 1–3)$ and $C_2$ oxygenates from syngas on different size of Cu clusters, including $Cu_{13}$, $Cu_{38}$ and $Cu_{55}$ clusters, has been performed to probe into the effect of Cu cluster size on the selectivity. Here, the results are obtained using DFT calculations. Our results show that the adsorption ability of the species involving in syngas conversion decreases with the increasing of cluster size, in which $Cu_{13}$ cluster presents the strongest adsorption ability due to more edge sites. For CO initial step, CHO formation is the most favorable on three Cu clusters. Then, starting from CHO, $CH_x(x = 1–3)$ species are abundant rather than $CH_3OH$ on $Cu_{13}$ cluster; whereas, $CH_2$ is the most favored $CH_x$ monomer on $Cu_{38}$ cluster, which competes with $CH_3OH$; however, on $Cu_{55}$ cluster, $CH_3OH$ prefers to be produced from syngas rather than the favored monomer $CH_x(x = 2,3)$ species, which is similar to the bulk Cu(111) surface. Namely, the selectivity of $CH_x(x = 1–3)$ species decrease with the increasing of cluster size. On the other hand, starting from the most favored $CH_x$ monomer, $C_2$ oxygenates formed by CO insertion into $CH_x$ are the dominant products on both $Cu_{13}$ and $Cu_{38}$ clusters, however, on $Cu_{55}$ cluster, $CH_4$ formation is more preferable than $C_2$ oxygenates, suggesting that the selectivity of $C_2$ oxygenates decreases with the increasing of cluster size due to the easy $CH_4$ formation, moreover, the size of $Cu_{55}$ cluster has presented a similar catalytic performance with Cu bulk surface. In general, among $Cu_{13}$, $Cu_{38}$ and $Cu_{55}$ clusters, the smaller the cluster size is, the higher the selectivity of $C_2$ oxygenates is, $Cu_{13}$ cluster exhibits the highest productivity and selectivity toward the formation of $C_2$ oxygenates, that is probably related to the high concentration of low-coordinated defect sites on small size Cu cluster, which results in the high productivity and selectivity toward $C_2$ oxygenates.

## Acknowledgments

This work is financially supported by the National Natural Science Foundation of China (No. 21476155, 21276003 and 21276171), the Natural Science Foundation of Shanxi Province (No. 2014011012-2), the Program for the Top Young Academic Leaders of Higher Learning Institutions of Shanxi, and the Top Young Innovative Talents of Shanxi.

## Appendix A. Supplementary data

Supplementary data associated with this article can be found, in the online version, at http://dx.doi.org/10.1016/j.apsusc.2017.02.164.

## References

[1] D.H. Mei, R. Rousseau, S.M. Kathmann, V.A. Glezakou, M.H. Engelhard, W. Jiang, C. Wang, M.A. Gerber, J.F. White, D.J. Stevens, Ethanol synthesis from syngas over Rh-based/$SiO_2$ catalysts: a combined experimental and theoretical modeling study, J. Catal. 271 (2010) 325–342.
[2] Y.M. Choi, P. Liu, Mechanism of ethanol synthesis from syngas on Rh(111), J. Am. Chem. Soc. 131 (2009) 13054–13061.
[3] W. Feng, Q.W. Wang, B. Jiang, P.J. Ji, Carbon nanotubes coated on silica gels as a support of Cu–Co catalyst for the synthesis of higher alcohols from syngas, Ind. Eng. Chem. Res. 50 (2011) 11067–11072.
[4] J. Sun, S.L. Wan, F. Wang, J.D. Lin, Y. Wang, Selective synthesis of methanol and higher alcohols over Cs/Cu/ZnO/$Al_2O_3$ catalysts, Ind. Eng. Chem. Res. 54 (2015) 7841–7851.
[5] M. Gupta, M.L. Smith, J.J. Spivey, Heterogeneous catalytic conversion of dry syngas to ethanol and higher alcohols on Cu-based catalysts, ACS Catal. 1 (2011) 641–656.
[6] Y.Y. Liu, K. Murata, M. Inaba, I. Takahara, K. Okabe, Mixed alcohols synthesis from syngas over Cs-and Ni-modified Cu/$CeO_2$ catalysts, Fuel 104 (2013) 62–69.
[7] Z.J. Zuo, L. Wang, Y.J. Liu, W. Huang, The effect of CuO–ZnO–$Al_2O_3$ catalyst structure on the ethanol synthesis from syngas, Catal. Commun. 34 (2013) 69–72.
[8] S.H. Yeon, D.H. Shin, N.S. Nho, K.H. Shin, C.S. Jin, S.C. Nam, Effect of support for alcohol-hydrocarbon synthesis from syngas in Cu-based catalyst, Korean J. Chem. Eng. 30 (2013) 864–870.
[9] N.D. Subramanian, G. Balaji, C.S.S.R. Kumar, J.J. Spivey, Development of cobalt–copper nanoparticles as catalysts for higher alcohol synthesis from syngas, Catal. Today 147 (2009) 100–106.
[10] J.C. Slaa, J.G. Van Ommen, J.R.H. Ross, The synthesis of higher alcohols using modified Cu/ZnO/$Al_2O_3$ catalysts, Catal. Today 15 (1992) 129–148.
[11] R. Xu, W. Wei, W.H. Li, T.D. Hu, Y.H. Sun, Fe modified $CuMnZrO_2$ catalysts for higher alcohols synthesis from syngas: effect of calcination temperature, J. Mol. Catal. A: Chem. 234 (2005) 75–83.

[12] R. Xu, C. Yang, W. Wei, W.H. Li, Y.H. Sun, T.D. Hu, Fe-modified $CuMnZrO_2$ catalysts for higher alcohols synthesis from syngas, J. Mol. Cata. A: Chem. 221 (2004) 51–58.
[13] N. Zhao, R. Xu, W. Wei, Y.H. Sun, $Cu/Mn/ZrO_2$ catalyst for alcohol synthesis by Fischer-Tropsch modified elements, React. Kinet. Catal. Lett. 75 (2002) 297–304.
[14] V. Mahdavi, M.H. Peyrovi, M. Islami, J.Y. Mehr, Synthesis of higher alcohols from syngas over $Cu-Co_2O_3/ZnO$, $Al_2O_3$ Catal. Appl. Catal. A: Gen. 281 (2005) 259–265.
[15] E. Fernández, M. Boronat, A. Corma, Trends in the reactivity of molecular $O_2$ with copper clusters: influence of size and shape, J. Phys. Chem. C 119 (2015) 19832–19846.
[16] Y. Okamoto, Density functional calculations of atomic and molecular adsorptions on 55-atom metal clusters: comparison with (111) surfaces, Chem. Phys. Lett. 405 (2005) 79–83.
[17] Y. Okamoto, Comparison of hydrogen atom adsorption on Pt clusters with that on Pt surfaces: a study from density-functional calculations, Chem. Phys. Lett. 429 (2006) 209–213.
[18] B.R. Cuenya, Synthesis and catalytic properties of metal nanoparticles: size shape, support, composition, and oxidation state effects, Thin Solid Films 518 (2010) 3127–3150.
[19] F.J.E. Scheijen, G.L. Beltramo, S. Hoeppener, T.H.M. Housmans, M.T.M. Koper, The electrooxidation of small organic molecules on platinum nanoparticles supported on gold: influence of platinum deposition procedure, J. Solid State Electr. 12 (2008) 483–495.
[20] M. Boronat, A. Leyva-Perez, A. Corma, Theoretical and experimental insights into the origin of the catalytic activity of subnanometric gold clusters: attempts to predict reactivity with clusters and nanoparticles of gold, Acc. Chem. Res. 47 (2014) 834–844.
[21] J.L. Fajin, A. Bruix, M.N. Cordeiro, J.R. Gomes, F. Illas, Density functional theory model study of size and structure effects on water dissociation by platinum nanoparticles, J. Chem. Phys. 137 (2012) 034701.
[22] Y.P. Xie, X.G. Gong, First-principles studies for CO and $O_2$ on gold nanocluster, J. Chem. Phys. 132 (2010), 244302-1-6.
[23] I.V. Yudanov, A. Genest, S. Schauermann, H.J. Freund, N. Rösch, Size dependence of the adsorption energy of CO on metal nanoparticles: a DFT search for the minimum value, Nano Lett. 12 (2012) 2134–2139.
[24] I.V. Yudanov, M. Metzner, A. Genest, N. Rösch, Size-dependence of adsorption properties of metal nanoparticles: a density functional study on palladium nanoclusters, J. Phys. Chem. C 112 (2008) 20269–20275.
[25] T.M. Soini, S. Krüger, N. Rösch, The DFT + U method and its application to the adsorption of CO on platinum model clusters, J. Chem. Phys. 140 (2014), 174709-1-9.
[26] M.B. Knickelbein, Electronic shell structure in the ionization potentials of copper clusters, Chem. Phys. Lett. 192 (1992) 129–134.
[27] O. Kostko, N. Morgner, M. Astruc Hoffmann, B. Von Issendorff, Photo electron spectra of $Na_n^-$ and $Cu_n^-$ with n = 20–40: observation of surprising similarities, Eur. Phys. J. D 34 (2005) 133–137.
[28] M.L. Zhang, G.P. Li, Energy and structure of copper clusters (n = 2–70, 147, 500) studied by the monte carlo method, Solid State Phenom. 121-123 (2007) 607–610.
[29] B.J. Winter, E.K. Parks, S.J. Riley, Copper clusters: the interplay between electronic and geometrical structure, J. Chem. Phys. 94 (1991) 8618–8621.
[30] Y.Z. Lu, W.T. Wei, W. Chen, Copper nanoclusters: synthesis: characterization and properties, Chin. Sci. Bull. 57 (2012) 41–47.
[31] G. Prieto, S. Beijer, M.L. Smith, M. He, Y. Au, Z. Wang, D.A. Bruce, K.P. De Jong, J.J. Spivey, P.E. De Jongh, Design and synthesis of copper-cobalt catalysts for the selective conversion of synthesis gas to ethanol and higher alcohols, Angew. Chem. Int. Ed. 53 (2014) 6397–6401.
[32] C.C. Lee, H.T. Chen, Ethylene epoxidation catalyzed by a $Cu_{38}$ nanoparticle: a computational study, J. Phys. Chem. C 120 (2016) 7646–7652.
[33] A. Karelovic, P. Ruiz, The role of copper particle size in low pressure methanol synthesis via $CO_2$ hydrogenation over Cu/ZnO catalysts, Catal. Sci. Technol. 5 (2015) 869–881.
[34] C. Liu, B. Yang, E. Tyo, S. Seifert, J. DeBartolo, B. Von Issendorff, P. Zapol, S. Vajda, L.A. Curtiss, Carbon dioxide conversion to methanol over size-selected $Cu_4$ clusters at low pressures, J. Am. Chem. Soc. 137 (2015) 8676–8679.
[35] Y. Yang, J. Evans, J.A. Rodriguez, M.G. White, P. Liu, Fundamental studies of methanol synthesis from $CO_2$ hydrogenation on Cu(111) Cu clusters, and Cu/ZnO(0001), Phys. Chem. Chem. Phys. 12 (2010) 9909–9917.
[36] Z.J. Zuo, L. Wang, P.D. Han, W. Huang, Insight into the size effect on methanol decomposition over Cu-based catalysts based on density functional theory, Comput. Theor. Chem. 1033 (2014) 14–22.
[37] P. Liu, J.A. Rodriguez, Water-gas-shift reaction on metal nanoparticles and surfaces, J. Chem. Phys. 126 (2007) 164705-1-8.
[38] J.A. Rodriguez, P. Liu, J. Hrbek, J. Evans, M. Perez, Water gas shift reaction on Cu and Au nanoparticles supported on $CeO_2(111)$ and ZnO(0001): Intrinsic activity and importance of support interactions, Angew. Chem. Int. Ed. 46 (2007) 1329–1332.
[39] S. Gautam, K. Dharamvir, N. Goel, $CO_2$ adsorption and activation over medium sized $Cu_n$(n = 7, 13 and 19) cluster: a density functional study, Comput. Theor. Chem. 1009 (2013) 8–16.
[40] F. Mehmood, J. Greeley, P. Zapol, L.A. Curtiss, Comparative density functional study of methanol decomposition on $Cu_4$ and $Co_4$ clusters, J. Phys. Chem. B 114 (2010) 14458–14466.
[41] J.S. Boschen, J. Lee, T.L. Windus, J.W. Evans, D.J. Liu, Size dependence of S-bonding on (111) facets of Cu nanoclusters, J. Phys. Chem. C 120 (2016) 10268–10274.
[42] B. Delley, From molecules to solids with the $DMol^3$ approach, J. Chem. Phys. 113 (2000) 7756–7764.
[43] B. Delley, An all-electron numerical method for solving the local density functional for polyatomic molecules, J. Chem. Phys. 92 (1990) 508–517.
[44] D.X. Tian, H.L. Zhang, J.J. Zhao, Structure and structural evolution of Ag(n = 3-22) clusters using a genetic algorithm and density functional theory method, Solid State Commun. 144 (2007) 174–179.
[45] C.G. Zhou, J.P. Wu, A. Nie, R.C. Forrey, A. Tachibana, H.S. Cheng, On the sequential hydrogen dissociative chemisorption on small platinum clusters: a density functional theory study, J. Phys. Chem. C 111 (2007) 12773–12778.
[46] N. Govind, M. Petersen, G. Fitzgerald, D. King-Smith, J. Andzelm, A generalized synchronous transit method for transition state location, Comp. Mater. Sci. 28 (2003) 250–258.
[47] T.A. Halgren, W.N. Lipscomb, The synchronous-transit method for determining reaction pathways and locating molecular transition states, Chem. Phys. Lett. 49 (1977) 225–232.
[48] J. Greeley, M. Mavrikakis, A first-principles study of surface and subsurface H on and in Ni(111): diffusional properties and coverage-dependent behavior, Surf. Sci. 540 (2003) 215–229.
[49] K. Shin, D.H. Kim, S.C. Yeo, H.M. Lee, Structural stability of AgCu bimetallic nanoparticles and their application as a catalyst: a DFT study, Catal. Today 185 (2012) 94–98.
[50] W.Y. Li, F.Y. Chen, A density functional theory study of structural, electronic, optical and magnetic properties of small Ag-Cu nanoalloys, J. Nanopart. Res. 15 (2013) 1–14.
[51] Ş. Erkoç, R. Shaltaf, Monte Carlo computer simulation of copper clusters, Phys. Rev. A 60 (1999) 3053–3057.
[52] M. Kabir, A. Mookerjee, A.K. Bhattacharya, Structure and stability of copper clusters: a tight-binding molecular dynamics study, Phys. Rev. A 69 (2004), 043203-1-10.
[53] J.P.K. Doye, D.J. Wales, Global minima for transition metal clusters described by Sutton–Chen potentials, New J. Chem. 22 (1998) 733–744.
[54] S. Darby, T.V. Mortimer-Jones, R.L. Johnston, C. Roberts, Theoretical study of Cu–Au nanoalloy clusters using a genetic algorithm, J. Chem. Phys. 116 (2002) 1536–1550.
[55] S. Özçelik, Z.B. Güvenç, Structures and melting of $Cu_n$ (n = 13, 14, 19, 55, 56) clusters, Surf. Sci. 532 (2003) 312–316.
[56] S. Nunez, R.L. Johnston, Structures and chemical ordering of small Cu-Ag clusters, J. Phys. Chem. C 114 (2010) 13255–13266.
[57] Y.H. Park, I.A. Hijazi, Critical size of transitional copper clusters for ground state structure determination: empirical and ab initio study, Mol. Simulat. 38 (2012) 241–247.
[58] R. Ferrando, A. Fortunelli, G. Rossi, Quantum effects on the structure of pure and binary metallic nanoclusters, Phys. Rev. B 72 (2005) 085449.
[59] I.A. Hijazi, Y.H. Park, Structure of pure metallic nanoclusters: Monte Carlo simulation and ab initio study, Eur. Phys. J. D 59 (2010) 215–221.
[60] M. Itoh, V. Kumar, T. Adschiri, Y. Kawazoe, Comprehensive study of sodium, copper, and silver clusters over a wide range of sizes $2 \leq N \leq 75$, J. Chem. Phys. 131 (2009) 174510.
[61] H.F. Gong, W. Lu, L.M. Wang, G.P. Li, S.X. Zhang, The effect of deposition velocity and cluster size on thin film growth by Cu cluster deposition, Comput. Mater. Sci. 65 (2012) 230–234.
[62] H.F. Gong, W. Lu, L.M. Wang, G.P. Li, Cluster size and substrate temperature affecting thin film formation during copper cluster deposition on a Si(001) surface, Chin. Phys. B 21 (2012) 113601.
[63] L. Zhang, W. Li, Molecular dynamics investigation to indicate facet effects on coalescence processes of two copper clusters with different structures, Comput. Mater. Sci. 51 (2012) 91–95.
[64] U. Lammers, G. Borstel, Electronic and atomic structure of copper clusters, Phys. Rev. B 49 (1994) 17360–17377.
[65] H.Y. Zheng, R.G. Zhang, Z. Li, B.J. Wang, Insight into the mechanism and possibility of ethanol formation from syngas on Cu(100) surface, J. Mol. Catal. A: Chem. 404 (2015) 115–130.
[66] R.G. Zhang, X.C. Sun, B.J. Wang, Insight into the preference mechanism of $CH_x$(x = 1–3) and C–C chain formation involved in $C_2$ oxygenate formation from syngas on the Cu(110) surface, J. Phys. Chem. C 117 (2013) 6594–6606.
[67] R.G. Zhang, G.R. Wang, B.J. Wang, Insights into the mechanism of ethanol formation from syngas on Cu and an expanded prediction of improved Cu-based catalyst, J. Catal. 305 (2013) 238–255.
[68] S.S.C. Chuang, R.W. Stevens, R. Khatri, Mechanism of $C_{2+}$ oxygenate synthesis on Rh catalysts, Top. Catal. 32 (2005) 225–232.
[69] J. Cheng, P. Hu, P. Ellis, S. French, G. Kelly, C.M. Lok, Chain growth mechanism in Fischer-Tropsch synthesis: a DFT study of C—C coupling over Ru Fe, Rh, and Re surfaces, J. Phys. Chem. C 112 (2008) 6082–6086.
[70] N. Kapur, J. Hyun, B. Shan, J.B. Nicholas, K. Cho, Ab initio study of CO hydrogenation to oxygenates on reduced Rh terraces and stepped surfaces, J. Phys. Chem. C 114 (2010) 10171–10182.
[71] L.C. Grabow, M. Mavrikakis, Mechanism of methanol synthesis on Cu through $CO_2$ and CO hydrogenation, ACS Catal. 1 (2011) 365–384.
[72] F. Studta, F. Abild-Pedersena, Q.X. Wu, A.D. Jensen, B. Temel, J.D. Grunwaldte, J.K. Nørskov, CO hydrogenation to methanol on Cu–Ni catalysts: theory and experiment, J. Catal. 293 (2012) 51–60.

[73] X.C. Sun, R.G. Zhang, B.J. Wang, Insights into the preference of $CH_x$(x = 1–3) formation from CO hydrogenation on Cu(111) surface, Appl. Surf. Sci. 265 (2013) 720–730.
[74] J.J. Spivey, A. Egbebi, Heterogeneous catalytic synthesis of ethanol from biomass-derived syngas, Chem. Soc. Rev. 36 (2007) 1514–1528.
[75] Y.H. Zhao, K.J. Sun, X.F. Ma, J.X. Liu, D.P. Sun, H.Y. Su, W.X. Li, Carbon chain growth by formyl insertion on rhodium and cobalt catalysts in syngas conversion, Angew. Chem. Int. Ed. 50 (2011) 5335–5338.
[76] J.B. Wang, Q. Sun, S. Chan, H.B. Su, The acceleration of methanol synthesis and $C_2$ oxygenates formation on copper grain boundary from syngas, Appl. Catal. A: Gen. 509 (2016) 97–104.
[77] C.M. Truong, J. Rodriguez, D.W. Goodman, CO adsorption isotherms on Cu(100) at elevated pressures and temperatures using infrared reflection absorption spectroscopy, Surf. Sci. 271 (1992) L385–L391.
[78] G.A. Beitel, C.P.M.D. Groot, H. Oosterbeek, J.H. Wilson, A combined in-situ PM-RAIRS and kinetic study of single-crystal cobalt catalysts under synthesis gas at pressures up to 300 mbar, J. Phys. Chem. B 101 (1997) 4035–4043.
[79] D.J. Elliott, F. Pennella, Effects of transition metals on CuZnO alcohol synthesis catalysts, J. Catal. 102 (1986) 464–466.
[80] D.J. Elliott, Higher alcohol synthesis over CuO/ZnO catalysts: relationship between methanol and higher alcohol syntheses, J. Catal. 111 (1988) 445–449.
[81] M. Behrens, F. Studt, I. Kasatkin, S. Kühl, M. Hävecker, F. Abild-Pedersen, S. Zander, F. Girgsdies, P. Kurr, B.L. Kniep, The active site of methanol synthesis over $Cu/ZnO/Al_2O_3$ industrial catalysts, Science 336 (2012) 893–897.
[82] T.H. Pham, Y.Y. Qi, J. Yang, X.Z. Duan, G. Qian, X.G. Zhou, D. Chen, W.K. Yuan, Insights into hägg iron-carbide-catalyzed Fischer–Tropsch synthesis: suppression of $CH_4$ formation and enhancement of C—C coupling on $\chi$-$Fe_5C_2$(510), ACS Catal. 5 (2015) 2203–2208.